PONTIFICIA UNIVERSIDAD CATÓLICA DEL PERÚ

FACULTAD DE CIENCIAS E INGENIERÍA

Efectos de dispersión lineal y advección por flujo externo en frentes en propagación

TRABAJO DE INVESTIGACIÓN PARA LA OBTENCIÓN DEL GRADO DE BACHILLER EN CIENCIAS CON MENCIÓN EN FÍSICA

AUTOR

Andrés Alfredo Martínez Rodríguez

ASESOR

Pablo Martin Vilela Proaño

Lima, Agosto, 2020

ET LUX IN TENEBRIS LUCET
MCMXVII

Abstract

Kuramoto-Sivashinsky equation in a two dimensional slab with infinite walls and advection by external flow is considered. Stationary front solutions were then found using the shooting method with simple Euler method and oscillatory front solutions were solved with simple Euler method. Numerical results for both were analyzed, finding the solutions for stationary fronts including external flow, Couette and Poiseuille. A modified Kuramoto-Sivashinsky equation, similar to the equation used to described solitary waves was also considered and the effect it had on stationary fronts with and without external flow was also explored. For oscillatory solutions, the front profiles and the phase space diagrams were calculated, a bifurcation diagram was also analyzed for no external flow as well as for fronts advected by Poiseuille and Couette external flow, and good agreement with Feigenbaum's number was found in all cases.

ET LUX IN TENEBRIS LUCET
MCMXVII

Contents

List of Figures

List of Tables

Chapter 1

Introduction

The Kuramoto-Sivashinsky equation appeared in the late 1970s, derived from the instabilities in laminar flames [2, 3], as a simplification of the reaction-diffusion equation. The reaction-diffusion equation has uses in several areas of research, such as chemistry, to model reaction-diffusion experiments and in combustion theory, biology [4], and several other fields. It has been thoroughly studied in these different fields since the early 20th century. As mentioned before, the Kuramoto-Sivashinsky equation emerged as a simplified version of the reaction-diffusion equation, and ever since it has been focused on by research extensively, with new information [5] being found now, and with applications to fields such as chemical reactions [6]. Variations of the Kuramoto-Sivashinsky equation have also been thoroughly studied, with periodic boundary conditions [7], Neumann boundary conditions [8], or other [9], even adding in new terms [10], using a modified Kuramoto-Sivashinsky equation [11, 12], as well as its similarities to the spatial behavior of other types of systems, such as the one dimensional non-linear maps [13], have been studied.

However, there is another equation that results in the Kuramoto-Sivashinsky equation. In the early 19th century, John Scott Russell proposed a model for a traveling wave in water[14]. This can be easily observed in nature, a drop of water on a larger body of water will create waves that travel with polar symmetry. Over a century later, when the use of computers to analyze more complex systems was becoming more prevalent, more and more research on solitary waves, or solitons, was being done. A 1978 article [15] used an equation similar to the Kuramoto-Sivashinsky equation to describe the behavior of long nonlinear waves traveling down an inclined plane on a viscous fluid. The difference is a term with β as a constant, if $\beta = 0$ then it becomes the Kuramoto-Sivashinsky equation. This term describes the linear dispersion [16] of the wave in the medium, meaning it describes the phase velocity or the spreading of the wave. Considering the case of water waves, linear dispersion describes how waves of different wavelengths travel at different propagation speeds, and in shallow-waters, the propagation speed is solely related on the amplitude of the wave. This linear dispersion term would also have an effect on the stability of the waves depending on the wave amplitude and the wavelength [10]. Solitons are heavily studied now, with applications in several fields, including optics [17], as they work extensively with waves, and biology [18].

In this work we will explore the behavior exhibited by reaction fronts confined between two parallel plates described by the Kuramoto-Sivashinsky equation with boundary conditions derived by Margolis et al. [9], solved with simple Euler method. We will consider two different types of external

flow, Poiseuille and Couette flow, as well as no external flow and the results will be compared to each other to see the effects each of these have on the spatiotemporal behavior. To start off, we analyze the stationary solutions for the Kuramoto-Sivashinsky equation using the shooting method. For Poiseuille and Couette external flow, the equation will also be solved using the shooting method. For stationary front solutions, we will also consider the term that describes solitary waves, which depends on a constant β, which we solve with shooting method for small values of the constant. Following that, the regions where there are oscillatory and chaotic solutions will be examined, then we explore these regions further by defining a phase space and showing the diagrams that the system presents, as well as calculating the Feigenbaum's constant for the bifurcation diagram obtained with the value for the separation of the plates and the minimum and maximum velocity that the system allows. Feigenbaum's constant is then compared to the original results of [19] to verify if the results for our system hold up.

Chapter 2

Equations of motion

Reaction-diffusion dynamical systems are mathematical models, which are now mainly used in the fields of chemistry to see the evolution of reaction-diffusion phenomena. This model exhibits very rich spatio-temporal behavior and has become popular in dynamical system study. When used in chemistry, it describes the change of concentration of different chemical substances. Could be reactants, which are used up in a chemical reaction, forming products that then spread over the space. Reaction-diffusion systems are described by the general equation, which in this case we will only consider in one dimension,

$$\frac{\partial \mathrm{z}}{\partial t} = \mathrm{F}(\mathrm{z}) + \mathrm{D}\Delta \mathrm{z}, \tag{2.1}$$

where z is a vector, that has the concentrations of the different substances as its components, F is a vector function that corresponds to the type of reaction the system undergoes and D is the diffusion matrix which is assumed to be diagonal [1]. After a series of simplifications and assumptions

[1, 20] we arrive at the Kuramoto-Sivashinsky equation

$$\frac{\partial H}{\partial T} = \nu\frac{\partial^2 H}{\partial X^2} + \frac{V_0}{2}\left(\frac{\partial H}{\partial X}\right)^2 - \kappa\frac{\partial^4 H}{\partial X^4}, \tag{2.2}$$

where the variables H and T describe the position of the front at time T, ν and κ are related to the diffusivities of the different reactants [21]. V_0 is the propagation speed of the front that the system allows.

2.1 Fronts described by Kuramoto-Sivashinsky equation

The Kuramoto-Sivashinsky equation, eq. 2.2 describes the front profile in a chemical reaction. In this work we will consider our system, the reactants and products, confined in a two dimensional (x and z axis) slab, confined by two infinite parallel plates, placed in $X = 0$ and $X = \tilde{L}$ as shown in fig. 2.1 . To be able to further analyze this equation and its behavior, a change to dimensionless units is necessary. We make this change by making use of the substitution of X, H and T: $X = L_x x$, $H = L_h h$ and $T = L_t t$, where x, h and t are dimensionless units, the x we are using corresponds to the reference system we place the parallel plates in. We assume that ν, κ are non-zero, we define $L_x = \sqrt{\kappa/|\nu|}$, $L_t = \kappa/\nu^2$, and $L_h = |\nu|/V_0$. Replacing all these substitutions in eq. 2.2, we obtain

$$\frac{\partial h}{\partial t} = \frac{|\nu|}{\nu}\frac{\partial^2 h}{\partial x^2} + \frac{1}{2}\left(\frac{\partial h}{\partial x}\right)^2 - \frac{\partial^4 h}{\partial x^4}, \tag{2.3}$$

where h describes the height of the front in the z-axis, at a time t. The coefficient of $\frac{\partial^2 h}{\partial x^2}$, $\frac{|\nu|}{\nu}$, can only have 2 values, -1 or 1. We will only consider

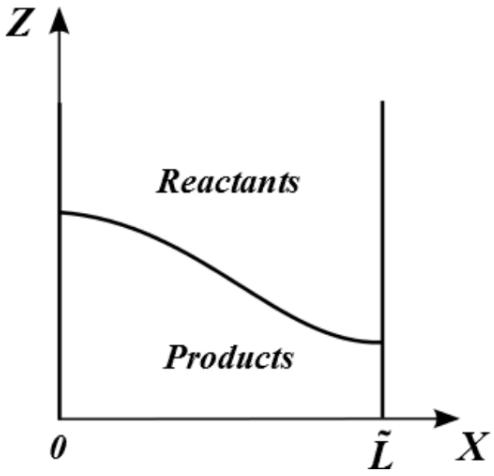

Figure 2.1: Graphic showing the front, reactants and products in our system [1].

it to be -1 seeing as Eq. 2.3 allows for flat front instabilities only when this coefficient is equal to -1 [21]. We will also consider boundary conditions set by Margolis et al. [9], $\frac{\partial h}{\partial x} = 0$ and $\frac{\partial^3 h}{\partial^3 x} = 0$ at our boundaries $x = 0$ and $x = L$.

2.1.1 Stationary fronts

We take eq. 2.3 and define a reference frame that moves together with the front described by the equation. This allows us to observe the front as if it is stationary. We impose that the solutions we are seeking have constant front velocity in the z-axis, and define the front height as a linear function of time, $h = h_0 - ct$ where h_0 is our stationary front profile, our constant front velocity, as well as the velocity of the reference frame, is c. Substituting our function for h in eq. 2.3 results in

$$-c = -\frac{\partial^2 h_0}{\partial x^2} + \frac{1}{2}\left(\frac{\partial h_0}{\partial x}\right)^2 - \frac{\partial^4 h_0}{\partial x^4}, \tag{2.4}$$

where h_0, x are the described above.

To solve eq. 2.4, in which our only unknowns are the constant front velocity c and the values of $\frac{\partial^2 h_0}{\partial x^2}$, we will make use of the shooting method [22]. To make use of this, we first split eq. 2.11 into four differential equations where each derivative will become a new variable:

$$\begin{cases} u = \frac{dh_o}{x} \\ v = \frac{du}{dx} \\ w = \frac{dv}{dx} \\ \frac{dw}{dx} = c - v + \frac{1}{2}u^2. \end{cases} \tag{2.5}$$

This system of equations contains two free parameters, which are the unknown values we have mentioned above, c and v at $x = 0$. Giving guessing values to these parameters, the system was solved using simple Euler method in order to reach the boundary at $x = L$, and following this our guessing values are adjusted to be able to fulfill the boundary conditions imposed at $x = L$. No significant difference between using simple Euler method and fourth order Runge-Kutta method to solve eq. 2.5. This method was implemented using a grid of 10000 points in x.

Linear dispersion

We will also add in another term to eq. 2.3 [10] for a more robust equation to test. This term turns the Kuramoto-Sivashinsky equation into an equation that describes the movement of long waves along a particular medium [10]. The effect this term has is describe the linear dispersion as the wave

is traveling along a medium at constant speed. The wave that travels maintains its form and is called a soliton [16]. We apply it in this case seeing as the propagating front that is being examined has constant speed. We plug in the term $\beta \frac{\partial^3 h_0}{\partial x^3}$ in eq. 2.4 and applying the same procedure of splitting the equation into a system of equations with new variables results in:

$$\begin{cases} u = \frac{dh_o}{x} \\ v = \frac{du}{dx} \\ w = \frac{dv}{dx} \\ \frac{dw}{dx} = c - v + \frac{1}{2}u^2 + \beta w. \end{cases} \tag{2.6}$$

This system of equations is solved using the shooting method with simple Euler like described before. The process is the same except that this time we first start off with $\beta = 0$ and from there we gradually begin increasing the value of β by small amounts and adjusting our guesses for c and v at $x = 0$ to fulfill the boundary conditions, this is done until we reach the desired value of β.

2.1.2 Oscillatory fronts

The other type of fronts we will study are oscillatory fronts. As their name implies, and, different from stationary fronts, these are fronts that oscillate between different solutions. Systems that exhibit this behavior also exhibit period doubling bifurcations, which is what we are interested in. There must be a parameter for which our setup shows this type of

behavior. Similar to the work of Smyrlis and Papageorgiou [13], we will be examining the average front velocity.

Contrary to stationary fronts, we expand h into a Fourier cosine series, we do this as the cosine series will easily fulfill the boundary conditions at $x = 0$ and $x = L$,

$$h(x,t) = \sum_{n=0} H_n(t)\cos(nqx), \tag{2.7}$$

where x is the position along the space between the parallel plates, the parameter q is given by $q = \pi/L$. Replacing our cosine series into eq. 2.3 and separating the different cosine coefficients, we obtain a set of differential equations for the evolution of our Fourier coefficients H_n. For n>0:

$$\frac{\partial H_n}{\partial t} = (nq)^2 H_n - (nq)^4 H_n + \frac{q^2}{4}\sum_{l=1}\sum_{p=1} lpH_l H_p(\delta_{n,|l-p|} - \delta_{n,l+p}) \tag{2.8}$$

and for H_0:

$$\frac{\partial H_0}{\partial t} = \frac{q^2}{4}\sum_{l=1} l^2 H_l^2. \tag{2.9}$$

The coefficient H_0 corresponds to the average front height along the domain $0 \leq x \leq L$, the derivative described in eq. 2.9 becomes the average front velocity.

Eqs. 2.8 and 2.9 are solved with simple Euler, with a spatial grid of 100 points in x and time step size of 0.001 [20], and considering the cosine series expansion with $n = 8$. There were no significant differences in using simple Euler or fourth order Runge-Kutta method, as well as no significant difference between using $n = 25$ and $n = 8$ for the cosine Fourier expansion. To be able to find higher period oscillatory solutions, the system was

evolved from period-one solutions to the desired period.

Feigenbaum's constant

The Feigenbaum's constant is a number that predicts the universal non-linear behavior and it could be applied to not only non-linear maps but other complex nonlinear systems [13]. Feigenbaum first presented this while studying the behavior of recursive system, the logistic map. The logistic map is a very simple system that exhibits rich behavior as its parameters vary. The one dimensional logistic map for population x is defined as:

$$x_{n+1} = rx_n(1 - x_n), \tag{2.10}$$

where x_n is the population at step n, x_{n+1} is the population at step $n+1$, and r is the growth parameter. The population x can vary in an interval of $[0,1]$, r can vary in an interval of $[0,4]$. This simple equation shows different behavior depending on the value of the growth parameter, such as multiple period doubling bifurcations into chaotic behavior [23] as we can see in fig. 2.2. Feigenbaum's constant for a one dimensional linear map is defined by

$$\delta = \lim_{n\to\infty} \frac{r_n - r_{n-1}}{r_{n+1} - r_n} = 4.6692016... \tag{2.11}$$

Each r_n being the earliest value of r that the system exhibits n-solutions. As we can see in fig. 2.2 there are different intervals of r for which we have n-solutions. This means that $r_n - r_{n-1}$ is equal to the length of the

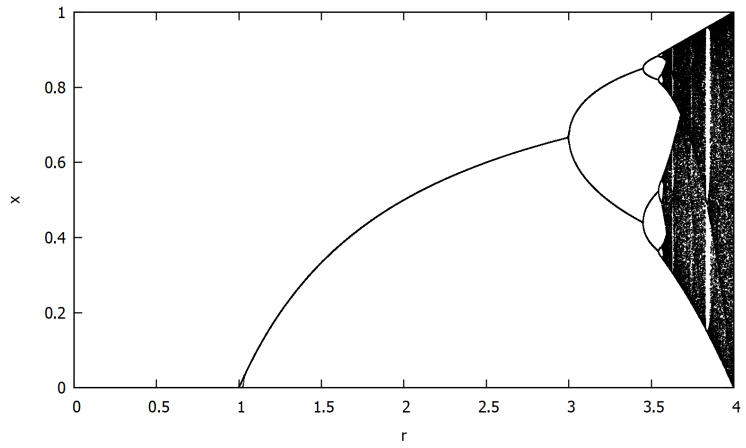

Figure 2.2: Bifurcation diagram of 2.10 for r ranging from 0 to 4.

interval for which there are n-solutions, and $r_{n+1} - r_n$ is equal to the length of the interval where there are n+1-solutions. For example, for period-two solutions, our length of interval r_n will be $r_2 - r_1$ and so on. Feigenbaum found that the nonlinear map presents a limit on the constant defined by eq. 2.11, which is 4.6692016 [19]. Since the Kuramoto-Sivashinsky equation also represents a complex nonlinear system, and exhibits period doublings, the Feigenbaum's constant should apply to it as well.

2.2 Fronts advected by external Poiseuille flow

First, when an external flow is considered in the system, we must add in a new term to eq. 2.3, which will correspond to the velocity profile of the external flow [24],

$$\frac{\partial h}{\partial t} = \frac{|v|}{v}\frac{\partial^2 h}{\partial x^2} + \frac{1}{2}\left(\frac{\partial h}{\partial x}\right)^2 - \frac{\partial^4 h}{\partial x^4} + V_z\Big|_{z=h}, \tag{2.12}$$

v_z is the profile of the external flow, which we will consider a Poiseuille flow. Considering the same setup as before, this flow is laminar, meaning

that the velocity at the plates less than the velocity in the halfway point of our x axis. The velocity profile of this flow is given by [20]:

$$V_z = \frac{6\bar{v}}{L^2}(L-x)x, \tag{2.13}$$

where $\bar{v}$ is the average velocity of the flow. As we are working with boundary conditions, the flow velocity profile also has to fulfill them. To do this, in a similar fashion to the steps taken for oscillatory fronts, eq. 2.13 is expanded into a Fourier cosine series, resulting in

$$V_z(x) = \sum_{n=0} V_n \cos(nqx), \tag{2.14}$$

with q previously defined as $q = \pi/L$, and V_n as the Fourier coefficients. The Fourier coefficients for the Poiseuille flow are given by

$$V_n = \begin{cases} -24\bar{v}/(n^2\pi^2), & \text{for } n \text{ even.} \\ 0, & \text{for } n \text{ odd.} \end{cases} \tag{2.15}$$

The difference between eq. 2.13 and eq. 2.14 is shown in fig. 2.3. The difference between using $n = 8$ and $n = 10$ was not significant up to 8 decimal places.

2.2.1 Stationary fronts advected by external Poiseuille flow

We add a new term to eq. 2.4 that corresponds to external Poiseuille flow. As discussed earlier, the velocity profile that describes this flow is eq. 2.13. Plugging in this term in eq. 2.4 results in:

$$-c = -\frac{\partial^2 h_0}{\partial x^2} + \frac{1}{2}\left(\frac{\partial h_0}{\partial x}\right)^2 - \frac{\partial^4 h_0}{\partial x^4} + \frac{6\bar{v}}{L^2}(L-x)\,x, \tag{2.16}$$

where $\bar{v}$ is the average velocity of the external flow, Poiseuille, in this case. Similarly to how we examined stationary profiles with no external flow, eq. 2.16 is split into a system of equations:

$$\begin{cases} u = \frac{dh_o}{x} \\ v = \frac{du}{dx} \\ w = \frac{dv}{dx} \\ \frac{dw}{dx} = c - v + \frac{1}{2}u^2 + \frac{6\bar{v}}{L^2}(L-x)\,x, \end{cases} \tag{2.17}$$

which is solved with the shooting method with c and v at $x = 0$ as free parameters. Giving guessing values to these parameters, the system was solved using simple Euler method in order to reach the boundary at $x = L$, and following this, our guessing values are adjusted to be able to fulfill the boundary conditions imposed at $x = L$. No significant difference between using simple Euler method and fourth order Runge-Kutta method to solve eq. 2.17 was found. This method was implemented using a grid of 10000 points in x.

Linear dispersion

We will also add in the solitary wave term to eq. 2.3. We plug in the term $\beta\frac{\partial^3 h_0}{\partial x^3}$ in eq. 2.16 and applying the same procedure of splitting the

equation into a system of equations with new variables results in:

$$\begin{cases} u = \frac{dh_o}{x} \\ v = \frac{du}{dx} \\ w = \frac{dv}{dx} \\ \frac{dw}{dx} = c - v + \frac{1}{2}u^2 + \beta w + \frac{6\bar{v}}{L^2}(L-x)x. \end{cases} \tag{2.18}$$

This system of equations is solved using the shooting method with simple Euler. No significant difference between simple Euler and fourth order Runge-Kutta was found. The process is the same except that this time we first start off with $\beta = 0$ and from there we gradually begin increasing the value of β by small amounts and adjusting our guesses for c and v at $x = 0$ to fulfill the boundary conditions, this is done until we reach the desired value of β.

2.2.2 Oscillatory fronts advected by external Poiseuille flow

For this we also work with the Fourier series expansion described in eq. 2.7. Including both our series expansion for V_z and the Fourier series expansion of h in in eq. 2.12 and grouping similar coefficients we arrive at

$$\frac{\partial H_n}{\partial t} = (nq)^2 H_n - (nq)^4 H_n + \frac{q^2}{4}\sum_{l=1}\sum_{p=1} lpH_l H_p(\delta_{n,|l-p|} - \delta_{n,l+p}) + V_n \tag{2.19}$$

and

$$\frac{\partial H_0}{\partial t} = \frac{q^2}{4}\sum_{l=1} l^2 H_l^2 + \bar{v}. \tag{2.20}$$

The coefficients H_n correspond to the different Fourier coefficients, $\bar{v}$ is the average flow velocity. In a similar manner to oscillatory fronts without external flow, eq. 2.20 corresponds to the average front velocity.

Eqs. 2.19 and 2.20 are solved using simple Euler, with a spatial grid of 100 points in x and time step size of 0.001, and a cosine expansion of $n = 8$. There were no significant differences in using simple Euler or fourth order Runge-Kutta method, as well as no significant difference between using $n = 25$ and $n = 8$ for the cosine Fourier expansion. To be able to find higher period oscillatory solutions, the system was evolved from period-one solutions to the desired period. What applies to oscillatory fronts with no external flow also apply to oscillatory fronts advected by external flow, thus we can find the Feigenbaum constant for this case.

2.3 Fronts advected by external Couette flow

The other type of flow we will explore is Couette flow. This type of flow consists of having one of the parallel plates moving at a constant speed, this could be in the same direction of the propagation of the front or in the opposite direction, while the other one remains stationary. This causes the substance between them to be advected by the difference in velocity of the parallel plates. The velocity profile for this type of flow is defined by

$$V_z = \frac{2\bar{v}}{L}(L - x), \tag{2.21}$$

or

$$V_z = \frac{2\bar{v}}{L}x, \tag{2.22}$$

where $\bar{v}$ is, likewise, the average flow velocity. We have not found significant differences when using either eq. 2.21 or 2.22 so we will only consider eq. 2.22 to be the velocity profile for the Couette flow. The same boundary conditions, derived by Margolis et al. [9] are imposed for Couette flow. A Fourier cosine expansion of eq. 2.22 is done to fulfill the boundary conditions, resulting in eq. 2.14, but with coefficients that follow

$$V_n = \begin{cases} -8\bar{v}/(n^2\pi^2), & \text{for } n \text{ odd.} \\ 0, & \text{for } n \text{ even.} \end{cases} \tag{2.23}$$

The difference between eq. 2.21 and the Fourier expansion with $n = 8$ is shown in fig. 2.4. We did not find significant differences between using $n = 8$ and $n = 10$ up to decimal places, so we will only consider $n = 8$.

2.3.1 Stationary fronts advected by Couette flow

A new term is added to eq. 2.4, that will describe external Couette flow. We plug in eq. 2.22, as no noticeable difference was found compared to using eq. 2.21,

$$-c = -\frac{\partial^2 h_0}{\partial x^2} + \frac{1}{2}\left(\frac{\partial h_0}{\partial x}\right)^2 - \frac{\partial^4 h_0}{\partial x^4} + \frac{2\bar{v}}{L}x, \tag{2.24}$$

where $\bar{v}$ is the average velocity of the external Couette flow. We split this into a system of first order differential equations, in the exact same

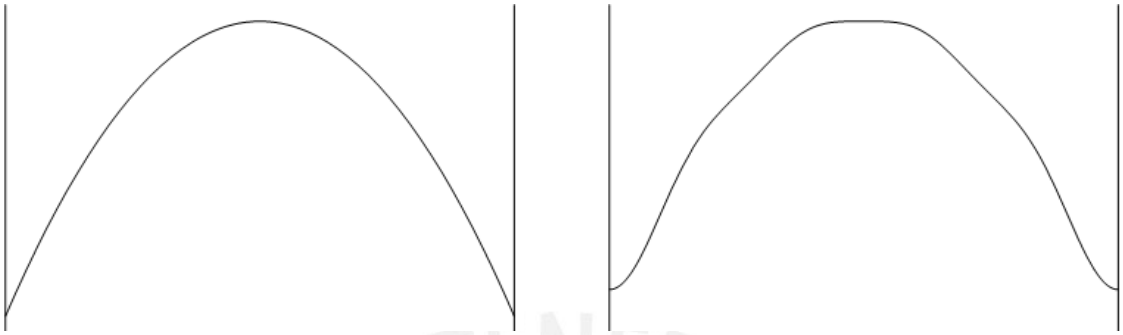

(a) (b)

Figure 2.3: Comparison between (a) eq. 2.13 and (b) eq. 2.14 with $n = 8$.

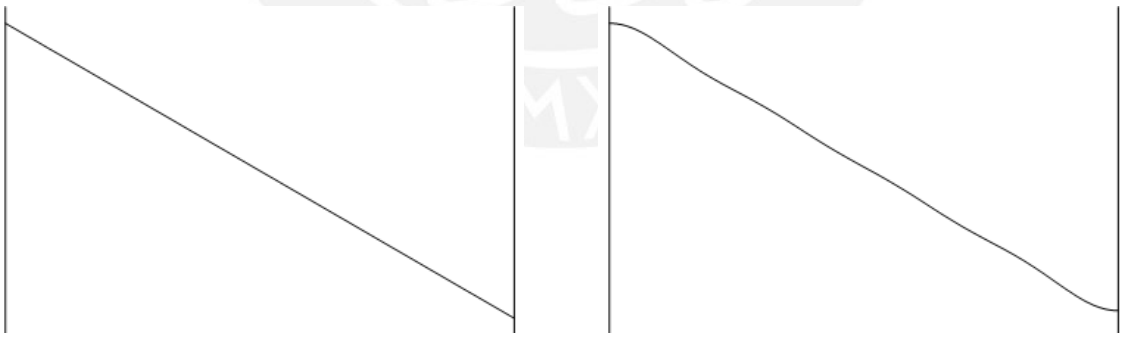

(a) (b)

Figure 2.4: Comparison between (a) eq. 2.21 and (b) eq. 2.14 with $n = 8$ for Couette flow considering eq. 2.23

manner as we have treated stationary solutions with no external flow and with external Poiseuille flow:

$$\begin{cases} u = \frac{dh_o}{x} \\ v = \frac{du}{dx} \\ w = \frac{dv}{dx} \\ \frac{dw}{dx} = c - v + \frac{1}{2}u^2 + \frac{2\bar{v}}{L}x, \end{cases} \tag{2.25}$$

which is solved with the shooting method with c and v at $x = 0$ as free parameters. With guessing values given to these parameters, the system was solved using simple Euler method in order to reach the boundary at $x = L$, and following this our guessing values are adjusted to be able to fulfill the boundary conditions imposed at $x = L$. No significant difference between using simple Euler method and fourth order Runge-Kutta method to solve eq. 2.17. This method was implemented using a grid of 10000 points in x.

Linear dispersion

We plug in the term $\beta \frac{\partial^3 h_0}{\partial x^3}$ in eq. 2.24 and applying the same procedure of splitting the equation into a system of equations with new variables results

in:

$$\begin{cases} u = \frac{dh_o}{x} \\ v = \frac{du}{dx} \\ w = \frac{dv}{dx} \\ \frac{dw}{dx} = c - v + \frac{1}{2}u^2 + \beta w + \frac{2\bar{v}}{L}x. \end{cases} \tag{2.26}$$

This system of equations is solved using the shooting method with simple Euler using v and c as free parameters. No significant difference between simple Euler and fourth order Runge-Kutta was found. We first start off with $\beta = 0$ and from there we gradually begin increasing the value of β by small amounts and adjusting our guesses for c and v at $x = 0$ to fulfill the boundary conditions, until we reach the desired value of β.

2.3.2 Oscillatory fronts advected by Couette flow

The cosine series expansion for h and the expansion for Couette flow, eq. 2.14 but considering eq. 2.23, are both plugged into eq. 2.12 resulting in

$$\frac{\partial H_n}{\partial t} = (nq)^2 H_n - (nq)^4 H_n + \frac{q^2}{4} \sum_{l=1} \sum_{p=1} lpH_l H_p (\delta_{n,|l-p|} - \delta_{n,l+p}) + V_n \tag{2.27}$$

and

$$\frac{\partial H_0}{\partial t} = \frac{q^2}{4} \sum_{l=1} l^2 H_l^2 + \bar{v}. \tag{2.28}$$

The coefficients H_n correspond to the different Fourier coefficients, $\bar{v}$ is the average flow velocity. In a similar manner to oscillatory fronts under external Poiseuille flow, eq. 2.28 corresponds to the average front velocity.

Eqs. 2.27 and 2.28 are solved using simple Euler, with a spatial grid of 100 points in x and time step size of 0.001, and a cosine expansion of $n = 8$. There were no significant differences in using simple Euler or fourth order Runge-Kutta method, as well as no significant difference between using $n = 25$ and $n = 8$ for the cosine Fourier expansion. To be able to find higher period oscillatory solutions, the system was evolved from period-one solutions to the desired period. We can also calculate the Feigenbaum constant for this case as the average front velocity causes the system to exhibit a behavior similar to the logistic map.

Chapter 3

Results

3.1 Stationary front solutions

3.1.1 Front height profiles

In this subsection we will only focus on the two branches, one of stable solutions and the other of unstable solutions. The front height profiles found for stationary solutions were similar to those found in oscillatory solutions, this is valid for no external flow and with external flow, both Poiseuille and Couette. The main effects of external Poiseuille flow and Couette flow are easily observed comparing the solid lines in figures 3.1 and 3.2. External Poiseuille flow tends to maintain the symmetry, or lack thereof, of the profile. If the profile is non-axisymmetric, as we can observe in fig. 3.1 (a), external Poiseuille flow tends to retain this non-axisymmetric behavior. When the profile is axisymmetric, external Poiseuille flow keeps it axisymmetric. External Couette flow, on the other hand, changes symmetric profiles to non-axisymmetric. The effect this type of external flow has on non-axisymmetric front height profiles is negligible, as the results

are also non-axisymmetric. As mentioned before, as we increase L and arrive at axisymmetric front height profiles and having those be advected by Couette flow results in non-axisymmetric front profiles. An explanation for this might be because of the symmetry the velocity profiles for each of the external flows we have tested, Poiseuille and Couette flow, present. Poiseuille flow presents an axisymmetric velocity profile, as shown in fig. 2.3, and Couette flow shows a non-axisymmetric velocity profile, shown in fig. 2.4, which correspond to the effects they have on axisymmetric front profiles.

We will only be considering positive values of β. The effects the term β has on front profiles is similar for no external flow and with external flow, be it Poiseuille or Couette. It changes the symmetry of the solutions, transforms axisymmetric fronts into non-axisymmetric fronts by increasing the front height in the right side of the profile and decreasing the front height in the left side, as we can observe in fig. 3.1. The same happens in the case of external flow, be it Poiseuille or Couette.

Linear dispersion

In fig. 3.3 only 2 branches are shown, these are the only ones we will consider for this part. As we can see, both branches overlap in the interval of $6.3 < x < 7.5$. As we begin to increase the value of β we can see how both branches start to diverge, the same effect as Poiseuille and Couette flow have on the branches. This is clearly observed in fig. 3.4. This behavior with β is also exhibited for the system under external flow, both Poiseuille

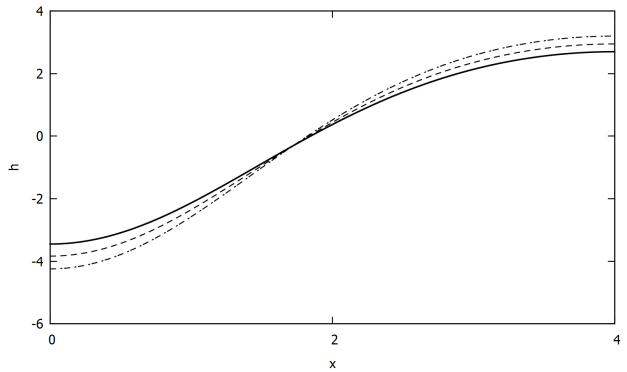

(a)

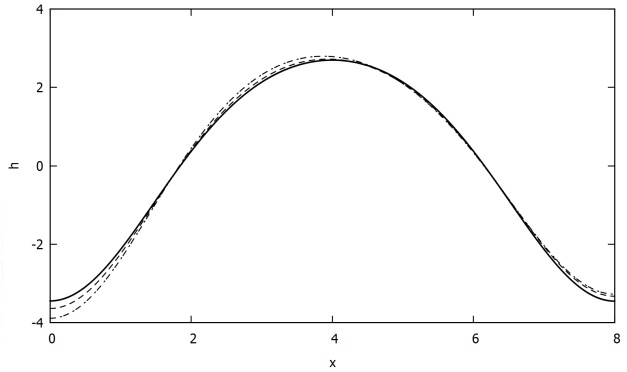

(b)

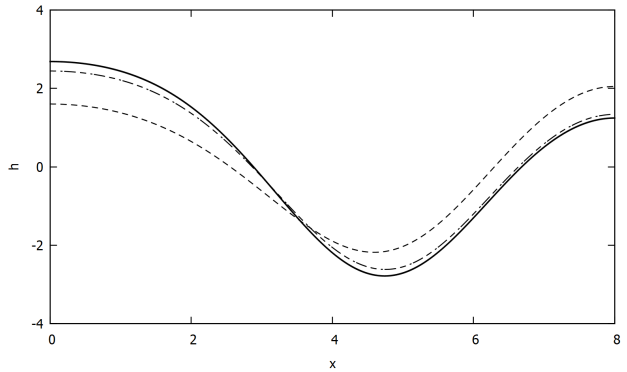

(c)

Figure 3.1: Front profiles, without external flow, for (a) $L = 4.0$ stable solution, (b) $L = 8.0$ stable solution, (c) $L = 8.0$ unstable solution. The solid line corresponds to $\beta = 0$, the dashed line is for $\beta = 0.1$ and the other dashed line with points corresponds to $\beta = 0.2$

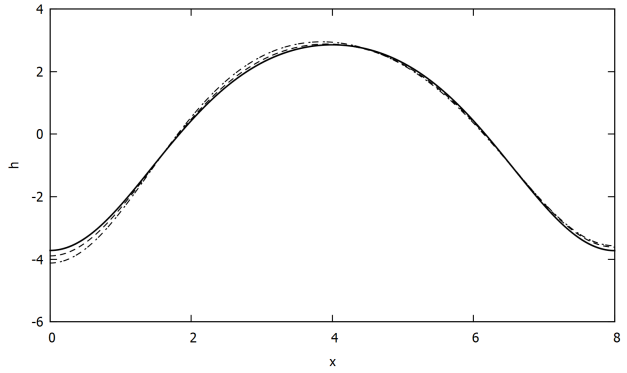

(a)

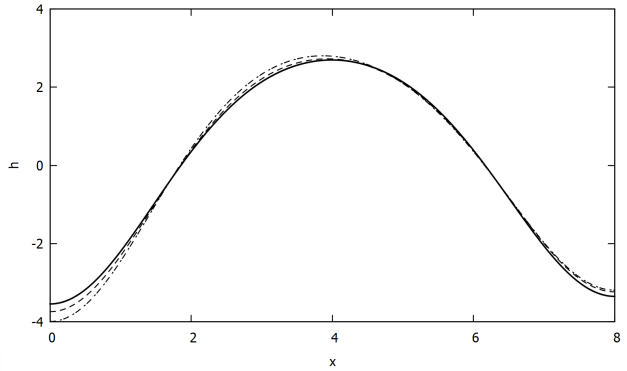

(b)

Figure 3.2: Front profiles, at $L = 8.0$, for (a) external Poiseuille flow with $\bar{v} = 0.2$, (b) external Couette flow with $\bar{v} = 0.2$.The solid line corresponds to $\beta = 0$, the dashed line is for $\beta = 0.1$ and the other dashed line with points corresponds to $\beta = 0.2$

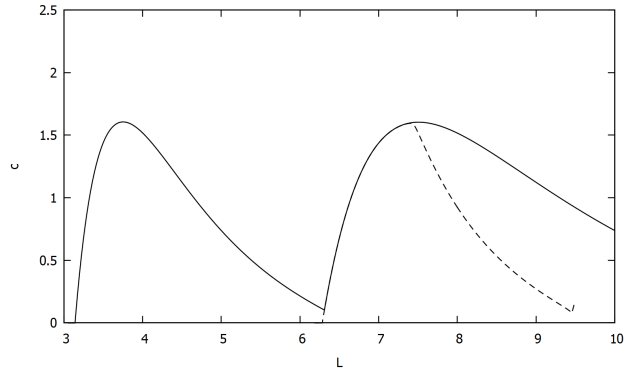

Figure 3.3: Values of c corresponding to each L. Both branches shown for no external flow. The solid line represents the stable solutions and the dashed line is for unstable solutions.

and Couette flow. In the case of no external flow, we can also observe how the β term tends to increase the maximum value for the branch of stable solutions and decrease the maximum value for the unstable solutions, this was also present for external flow, both Poiseuille and Couette. The main difference is that Couette flow reduces the unstable solutions to 0, which is not present in the system under no external flow or under Poiseuille external flow.

3.2 Oscillatory front solutions

3.2.1 Front height profiles

The front height profiles obtained change according to L. As we can see in fig. 3.5, for $L < 6$ the solutions are asymmetric. To further examine this behavior, we have increased the time we let the system evolve until $t = 1000000$ as compared to $t = 300$ shown in figs. 3.5, 3.6 and 3.7, for example, and noticed no significant difference, the behavior was the same. As we increase L the solutions become axisymmetric, as shown by the solutions for $L = 8$ in fig. 3.6. Increasing L further lets us arrive at asymmetric solutions once again, as shown in fig. 3.7 and oscillate between them. As we keep increasing L, we can observe, solutions become less and less symmetric and organized, we then arrive at a value of L where the front height exhibits more erratic behavior, as we can see in fig. 3.8, where the solutions shows four points of inflection. The behavior of the oscillating solutions can be seen in further depth on fig. 3.9, where we can clearly see

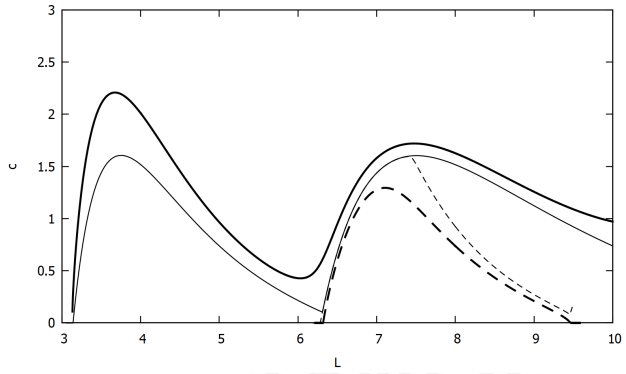

(a)

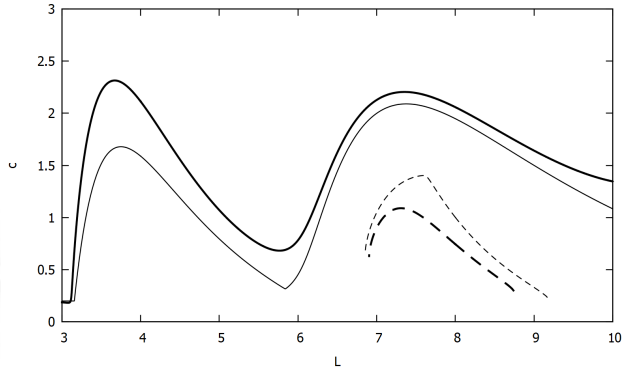

(b)

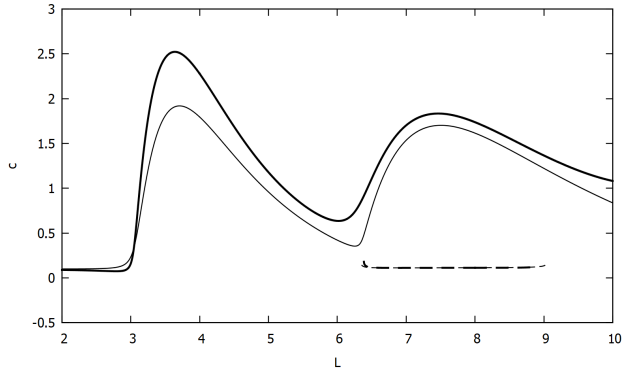

(c)

Figure 3.4: Values of c corresponding to each value of L. The solid lines correspond to stable solutions and dashed lines correspond to unstable front solutions. The thin line is for $\beta = 0$ and the thicker line is for $\beta = 0.2$. (a) corresponds to no external flow, (b) is for external Poiseuille flow and (c) is for external Couette flow.

that it oscillates between two solutions with a period of around $T = 25$. We can also observe that the same pattern of solutions are shown when the system is under external Couette flow and Poiseuille flow.

3.2.2 Average front velocity

We will not focus on $L < 8.65$ as the solutions have average velocity of period-one. The average front velocity, which is the characteristic mainly affected by external flow, exhibits a similar behavior to the front height, and it changes over time. As for no external flow, $\bar{v} = 0$, we can observe how the average front velocity, from eq. 2.8 we can build a formula for our average front velocity, v_{avg} at certain time t with simple Euler method

$$v_{avg} = \frac{dH_0}{dt}. \tag{3.1}$$

We can observe that the relationship between the average front velocity and time t is that of a sinusoidal curve as shown in fig. 3.10. As we further increase the value of L we can see several period doubling. The first one occurs at $L = 9.004$, in fig. 3.11 we can see that there are two sinusoidal curves with different amplitude, this is what we mean by period doubling here, there are new maxima and minima that appear. Period-8 at $L = 9.02$, and as we can observe in fig. 3.12, there are four local maxima and four local minima. As L becomes greater than 9.022 the system exhibits chaotic behavior. As we can see in fig. 3.13, there are several values of the local maxima and minima, which show little relation to the local maxima and

minima for the maxima and minima of previous values L. In the case of Poiseuille flow, $\bar{v}$ could be positive or negative and that determines part of the behavior of the average velocity of the front. As we can see in fig. 3.14, when $\bar{v} = -0.3$ the values of L for the period 4, 8 and chaotic behavior are $L = 9.38$, $L = 9.4$ and $L = 9.405$ respectively. When $\bar{v} > 0$, as shown in fig. 3.15, in this case $\bar{v} = 0.2$ the region where the period doubling occurs has become much smaller, $L = 8.989$, $L = 9.004$ and $L = 9.006$ for period 2, 4 and chaotic behavior. For Couette flow, we found no difference between positive and negative values of the flow velocity. For small values of the flow velocity, for example $\bar{v} = 0.2$, as shown in fig. 3.16, we observe that the upper branch of bifurcation diagram has been flattened. The values of L for period 4, period 8 and chaotic behavior are $L = 9.004$, $L = 9.02$ and $L = 9.022$ respectively.

Feigenbaum's constant

By using the definition of Feigenbaum's constant from eq. 2.11, we can calculate it for our system. First we do it with no external flow. Shown in table 3.1, we can see how the ratio of lengths trends towards 4,66. We can't calculate the rest as the system exhibits chaotic behavior making it impossible to know the exact period it is in. We can see how the values for the ratio trend towards 4.66 or close to it, if we were able to calculate more periods and more accurately these would certainly result in values close to the Feigenbaum's constant. This is in good agreement to other research involving Kuramoto-Sivashinsky equation [13], even in the presence

Interval length	Period	Ratio of lengths
0.3542	2	-
0.0153	4	23.150327
0.00251	8	6.095618
0.00052	16	4.826923
0.0025	Chaotic	-

Table 3.1: Feigenbaum's constant, ratio of interval lengths between solutions of different periods, calculation for no external flow.

Interval length	Period	Ratio of lengths
0.4844	2	-
0.02591	4	18.6955
0.0046	8	5.63261
0.00091	16	5.05494
0.00815	Chaotic	-

Table 3.2: Feigenbaum's constant, ratio of interval lengths between solutions of different periods, calculation for external Poiseuille flow with $\bar{v} = -0.3$.

of external flow as we can observe in tables 3.2 and 3.3.

3.2.3 Phase space

We define our phase space by fixing a point in the 100 grid on the x axis, observing the value of the front height at said point and the average front velocity. The results for the different periods with no external flow are shown in fig. 3.17. The other values of x and their respective phase space graphs have not been included as their behavior is similar to the other graphs. The phase space graphs for Poiseuille flow and Couette flow can

Interval length	Period	Ratio of lengths
0.46458	2	-
0.02156	4	21.54839
0.00381	8	5.65879
0.00086	16	4.43023
0.01112	Chaotic	-

Table 3.3: Feigenbaum's constant, ratio of interval lengths between solutions of different periods, calculation for external Couette flow with $\bar{v} = 0.2$.

be found at fig. 3.18 and 3.19 respectively. All of these were checked by letting the system evolve to $t = 1000000$ and we found that the same behavior was exhibited.

We can observe how the attractor in the phase space changes as the system exhibits chaotic behavior in both no external flow and in the presence of external flow, be it Poiseuille and Couette. As for no external flow, we found that the symmetry of the system could be observed in the phase space. The attractors corresponding to the points 0 and 100, 20 and 80, 40 and 60, were very similar. This started to change as the system kept undergoing more period doubling, and no symmetry after the system was under chaotic behavior. Similar behavior was found for positive and negative Poiseuille external flow, and in a similar manner, the symmetry was lost after undergoing continuous period doubling into chaotic behavior. This was not the case for external Couette flow, the symmetry was not as pronounced as for no external flow or Poiseuille flow, it was only noticed in some cases and only during period-2 solutions. After those, no such symmetry was able to be observed. This might be due to how the velocity profile for the different flows are, symmetric for Poiseuille flow and asymmetric for Couette flow. We can also observe how the no external flow attractors seem less erratic than those with external flow, especially Poiseuille flow.

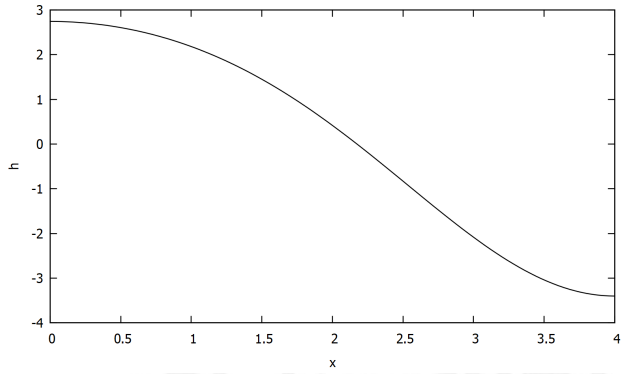

Figure 3.5: Front height profile for $\bar{v} = 0$, $L = 4.0$ at $t = 300$.

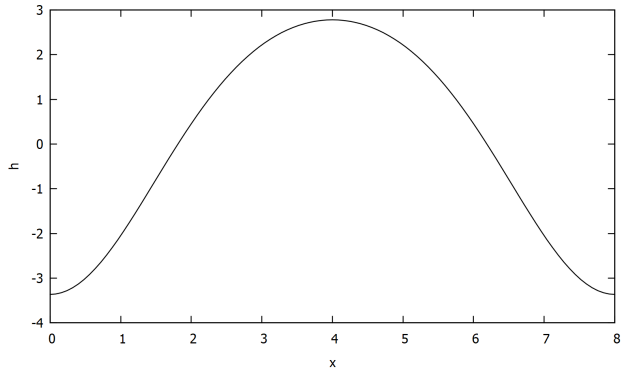

Figure 3.6: Front height profile for $\bar{v} = 0$, $L = 8.0$ at $t = 300$.

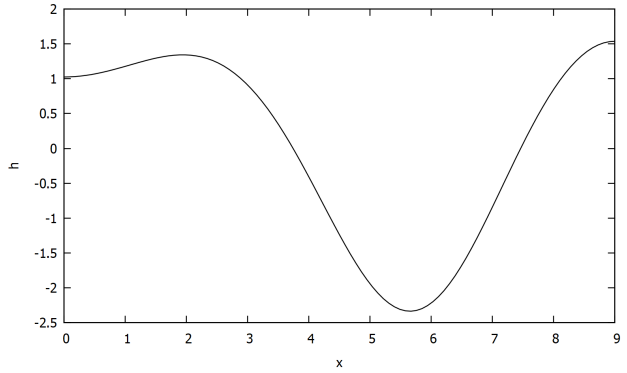

(a)

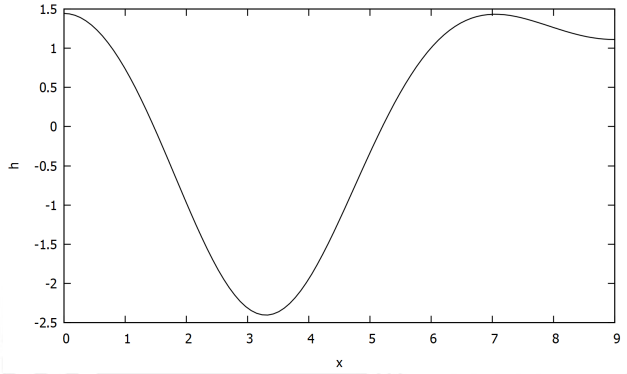

(b)

Figure 3.7: Front height profile for $\bar{v} = 0$, $L = 9.0$ at (a) $t = 300$ and (b) $t = 312$.

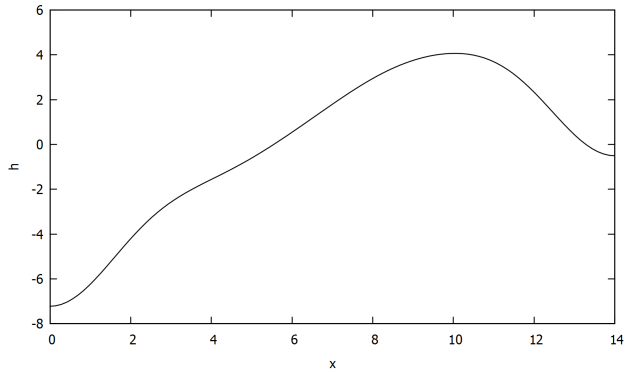

Figure 3.8: Front height profile for $\bar{v} = 0$, $L = 14.0$ at $t = 300$.

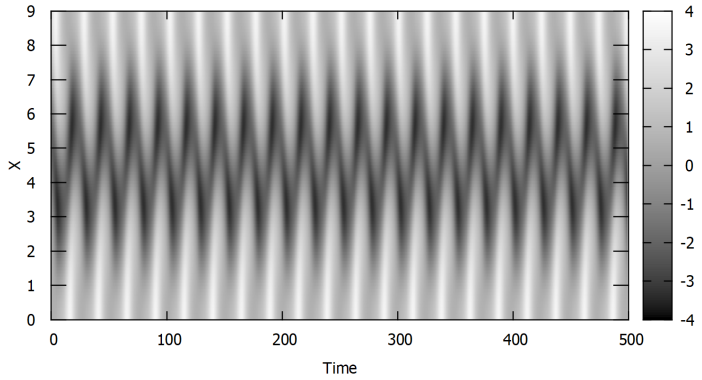

Figure 3.9: Front height at each point in x compared to the average height for $\bar{v} = 0$ at time t, $L = 9.0$.

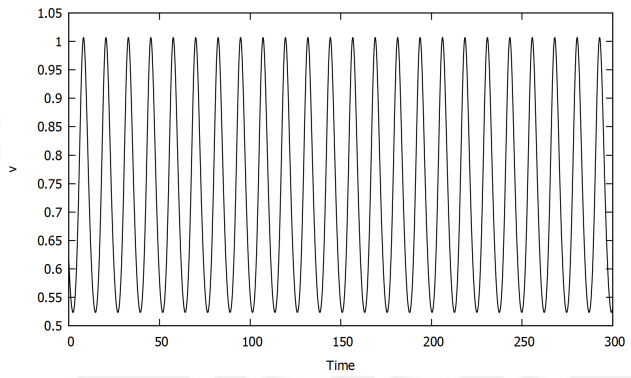

Figure 3.10: Average front velocity for $\bar{v} = 0$ and $L = 9.0$ at time t.

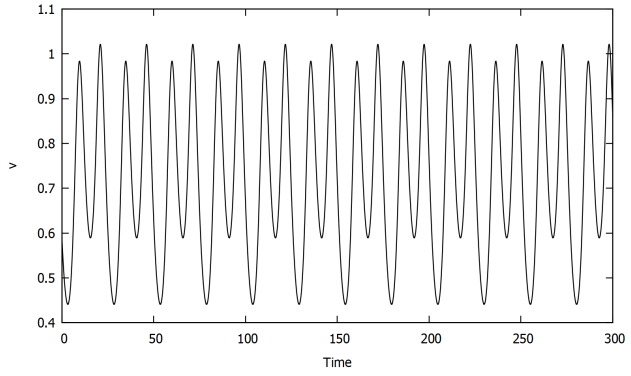

Figure 3.11: Average front velocity for $\bar{v} = 0$ and $L = 9.01$ at time t.

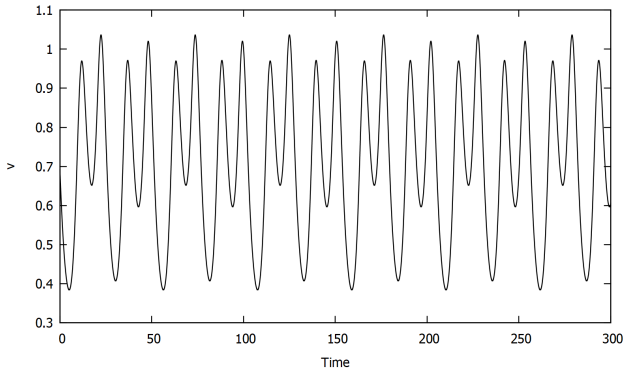

Figure 3.12: Average front velocity for $\bar{v} = 0$ and $L = 9.021$ at time t.

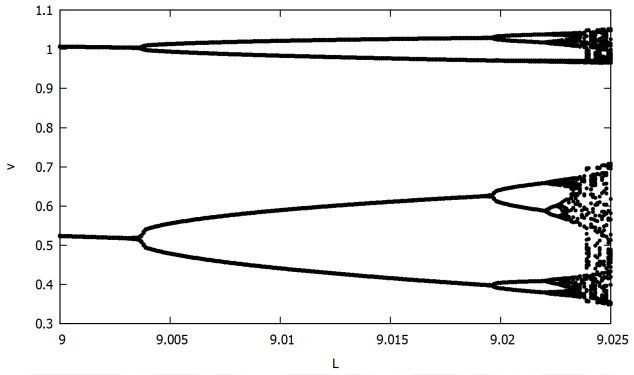

Figure 3.13: Maxima and minima for the average front velocity.

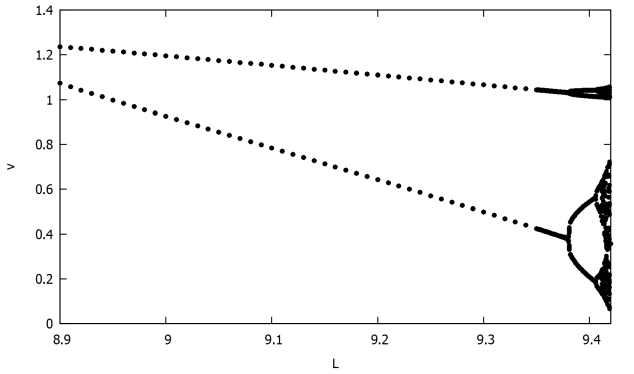

Figure 3.14: Maxima and minima for the average front velocity for external Poiseuille flow with $\bar{v} = -0.3$.

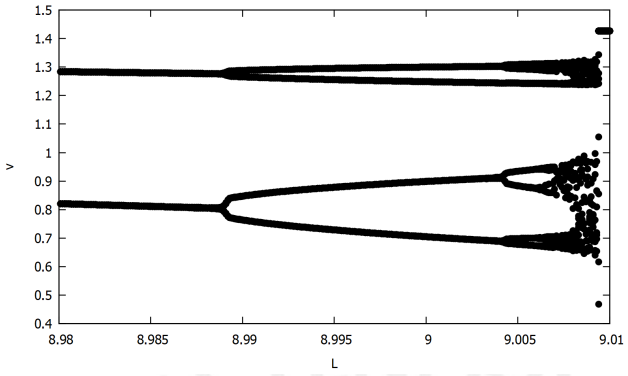

Figure 3.15: Maxima and minima for the average front velocity for external Poiseuille flow with $\bar{v} = 0.2$.

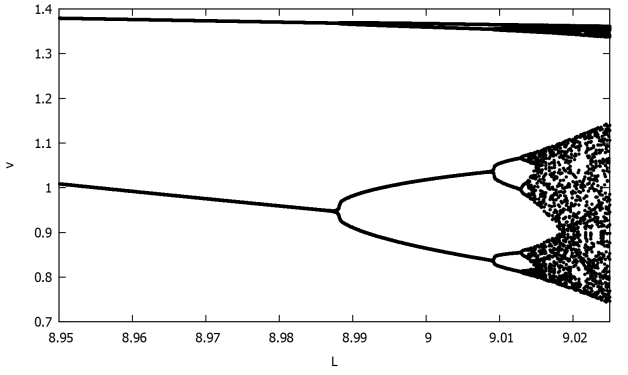

Figure 3.16: Maxima and minima for the average front velocity for external Couette flow with $\bar{v} = 0.2$.

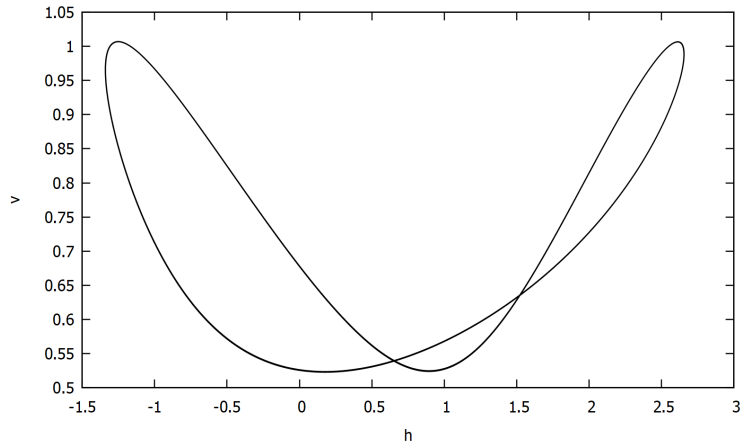

(a)

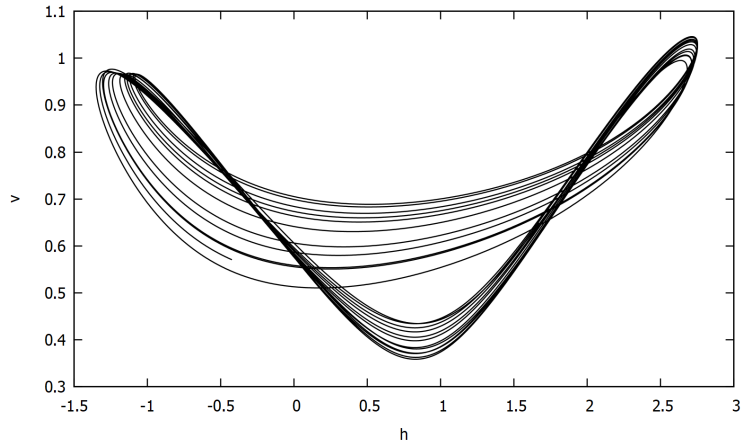

(b)

Figure 3.17: Phase space graph when $\bar{v} = 0$ and point 20 out of the 100 grid for (a) $L = 9.0$ and (b) $L = 9.025$.

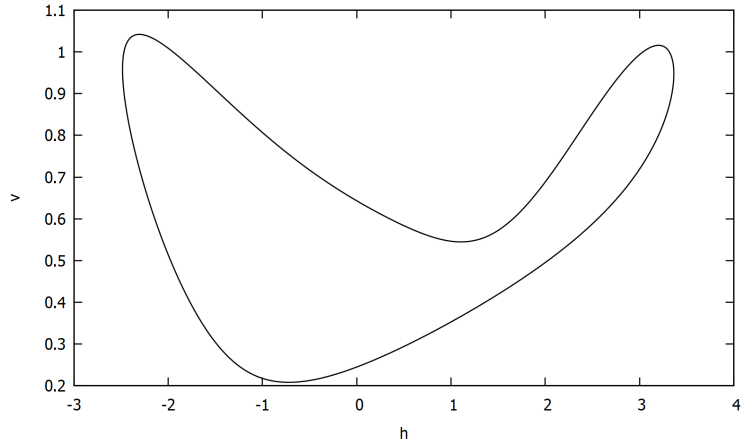

(a)

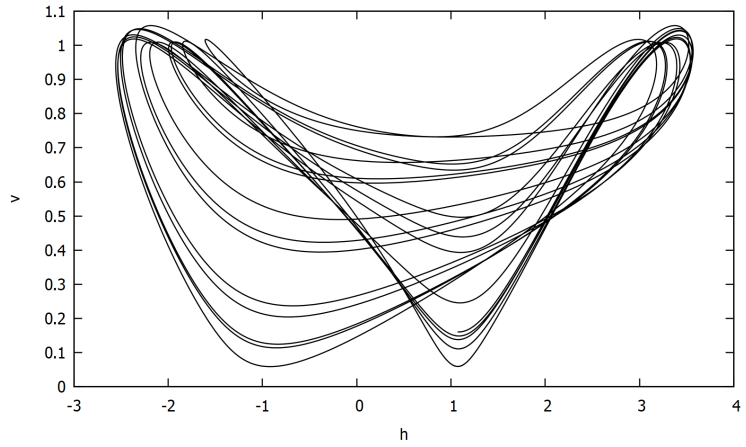

(b)

Figure 3.18: Phase space graph when Poiseuille flow has $\bar{v} = -0.3$ and point 20 out of the 100 grid for (a) $L = 9.4$ and (b) $L = 9.42$.

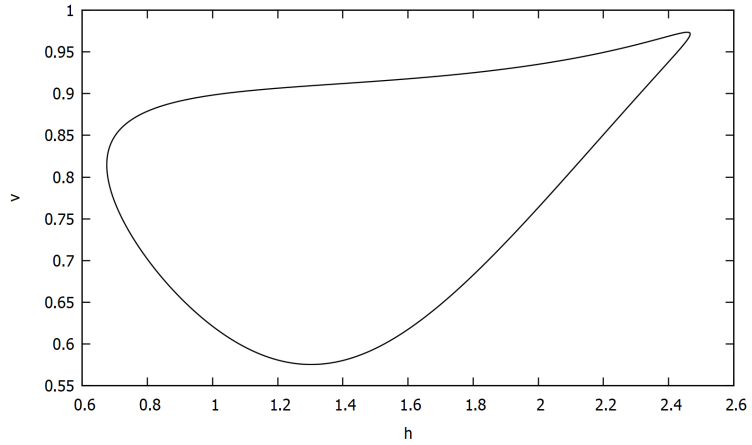

(a)

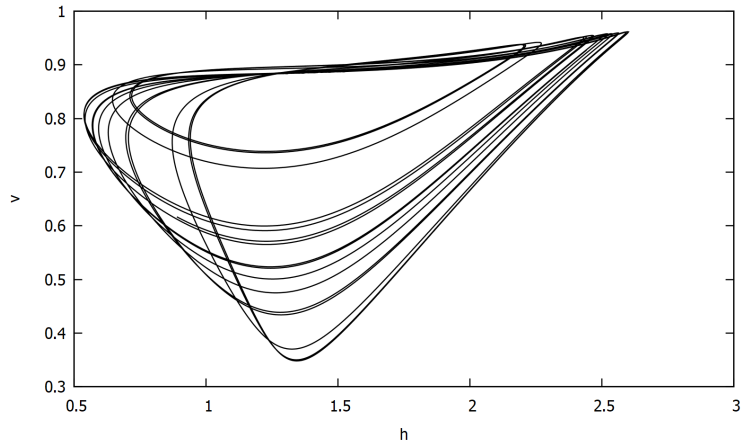

(b)

Figure 3.19: Phase space graph when Couette flow has $\bar{v} = -0.2$ and point 20 out of the 100 grid for (a) $L = 9.0$ and (b) $L = 9.025$.

Chapter 4

Conclusions and discussion

As for stationary solutions, we found that external flow tends to separate the branches that overlapped when there was no external flow present. The new term we added also separated these branches. Our results found that the β term always had the same effect, for all three cases of external flow. In all of these it tended to increase the values for the front height for values of x close to L and decrease the front height for values of x closer to 0. An immediate effect of this is that it will change the symmetry of the front, turning axisymmetric solutions into non-axisymmetric. Non-axisymmetric solutions underwent no change, as they all kept their non-axisymmetric characteristic. As mentioned before, this extra term added to the Kuramoto-Sivashisnky equations changes it to describe the movement of solitary waves, or solitons, and some of these solitons have a very defined shape. One of them, as we can observe in [10], has some similarities with the non axisymmetric front solution that belongs to $L = 4$, as we can see in fig. 3.1 (a). Coincidentally, out of all the front profiles examined with a small β term, this was the only one that maintains and will

maintain its form as we further increase the value of β. We can observe in the front profiles for $L = 8$ how, since one end is decreasing in h and the other is increasing in h this will make them seem similar to the front for $L = 4$. We can say that the solitary wave term is changing the form of our solutions to the form of a common one. The change in the front speed c and β can also be observed, with different effects on stable and unstable fronts, increasing c for stable fronts while decreasing it for unstable fronts. Further research of the effect of the solitary wave equation including external flow and its relationship to the stationary fronts can be done with bigger values of β as well as front solutions with different stability, seeing as we only analyzed two branches of solutions.

As we have mentioned before, we checked the results for no external flow and for Poiseuille external flow with results obtained by [20] with favourable results, from this we can determine that the algorithm is accurate enough for our different tests. The results we obtained for the front height profile for the different values of L, compare favorably to results for front height profiles obtained by Vilela [1] even if we are examining oscillating fronts, while [20] explores stationary fronts. We can also observe that external Couette flow had an effect on the upper branch shown in fig. 3.16 only, the values of L where the period doubling occurs stay the same as the results we obtained for no external flow, while when we have external Poiseuille flow, it has an effect on the length of the interval where we have period-two, four, and so on, solutions. We have also observed that when $\bar{v} > 0.3$ for Couette flow, the period doubling disappears altogether,

then it possibly has an effect on the lower branch as well. We have also found that the Feigenbaum's constant also held up for our tests, even after adding in a term corresponding to external flow. Meaning that even an equation as complex as the Kuramoto-Sivashinsky has similarities to the one dimensional linear map, which is one of the most simple equations that present chaotic behavior. For the phase space diagrams, we can observe how for no external flow and non chaotic solutions the height and velocity values accepted by the system follows only a particular set of values, as compared to chaotic solutions which accept a wide range of values. However, for the chaotic solution, we can see that there are some values that are close together. This we can see in all but the external Poiseuille flow of the chaotic phase space diagrams. It is better shown in fig. 3.19(b), in the upper side of the curve. So even if we can observe erratic behavior, it is also easily seen that it still follows some type of pattern, as shown from the phase space diagrams. The other bifurcations, that happens in regions where L is greater than the interval we have considered can also be further analyzed, as well as the phase diagrams for those, to see if every interval presents the same pattern, where Couette and Poiseuille external flow will present a more complex attractor than the solutions for no external flow.

Bibliography

[1] P. Vilela, 2015. Tesis Doctoral, Pontificia Universidad Católica del Perú. URL http://hdl.handle.net/20.500.12404/6345.

[2] G. Sivashinsky, 1977. "Nonlinear analysis of hydrodynamic instability in laminar flames—i. derivation of basic equations". Acta Astronautica 4(11):1177 . ISSN 0094-5765. URL http://www.sciencedirect.com/science/article/pii/0094576577900960.

[3] G. I. Sivashinsky, 1980. "On flame propagation under conditions of stoichiometry". SIAM Journal on Applied Mathematics 39(1):67. https://doi.org/10.1137/0139007, URL https://doi.org/10.1137/0139007.

[4] S. Petrovskii, 2009. "Reaction–diffusion waves in biology". Physics of Life Reviews 6:267.

[5] J. Liu, et al., 2018. "New exact solutions for the generalized kuramoto-sivashinsky equation". En "2018 Chinese Control And Decision Conference (CCDC)", págs. 2444–2447.

[6] R. Guzman, et al., 2018. "Fronts described by the kuramoto–sivashinsky equation under surface tension driven flow". The Euro-

pean Physical Journal Special Topics 227(5):521. ISSN 1951-6401. URL https://doi.org/10.1140/epjst/e2018-00126-y.

[7] D. Armbruster, et al., 1989. "Kuramoto–sivashinsky dynamics on the center–unstable manifold". SIAM Journal on Applied Mathematics 49(3):676. https://doi.org/10.1137/0149039, URL https://doi.org/10.1137/0149039.

[8] B. Nicolaenko, et al., 1985. "Some global dynamical properties of the kuramoto-sivashinsky equations: Nonlinear stability and attractors". Physica D: Nonlinear Phenomena 16(2):155 . ISSN 0167-2789. URL http://www.sciencedirect.com/science/article/pii/0167278985900569.

[9] S. B. Margolis, G. I. Sivashinsky, 1984. "Flame propagation in vertical channels: Bifurcation to bimodal cellular flames". SIAM Journal on Applied Mathematics 44(2):344. https://doi.org/10.1137/0144024, URL https://doi.org/10.1137/0144024.

[10] N. A. Kudryashov, E. D. Zargaryan, 1996. "Solitary waves in active-dissipative dispersive media". Journal of Physics A: Mathematical and General 29(24):8067. URL https://doi.org/10.1088%2F0305-4470%2F29%2F24%2F029.

[11] A. J. Bernoff, A. L. Bertozzi, 1995. "Singularities in a modified kuramoto-sivashinsky equation describing interface motion for phase transition". Physica D: Non-

linear Phenomena 85(3):375 . ISSN 0167-2789. URL http://www.sciencedirect.com/science/article/pii/0167278995000548.

[12] G. Akrivis, et al., 2012. "Computational study of the dispersively modified kuramoto–sivashinsky equation". SIAM Journal on Scientific Computing 34(2):A792. https://doi.org/10.1137/100816791, URL https://doi.org/10.1137/100816791.

[13] Y. Smyrlis, D. Papageorgiou, 1992. "Predicting chaos for infinite dimensional dynamical systems: The kuramoto- sivashinsky equation, a case study". Proceedings of the National Academy of Sciences of the United States of America 88:11129.

[14] A. T. Filippov, 2010. The Great Solitary Wave of John Scott Russell, Birkhäuser Boston, Boston, págs. 23–37. ISBN 978-0-8176-4974-6. URL https://doi.org/10.1007/978-0-8176-4974-6_2.

[15] J. Topper, T. Kawahara, 1978. "Approximate equations for long nonlinear waves on a viscous fluid". Journal of the Physical Society of Japan 44(2):663. https://doi.org/10.1143/JPSJ.44.663, URL https://doi.org/10.1143/JPSJ.44.663.

[16] A.-M. Wazwaz, 2009. Solitary Waves Theory. Springer Berlin Heidelberg, Berlin, Heidelberg. ISBN 978-3-642-00251-9, 479–502 págs. URL https://doi.org/10.1007/978-3-642-00251-9_12.

[17] M. Segev, et al., 1992. "Spatial solitons in photorefractive media". Phys. Rev. Lett. 68:923. URL https://link.aps.org/doi/10.1103/PhysRevLett.68.923.

[18] Z. Sinkala, 2006. "Soliton/exciton transport in proteins". Journal of Theoretical Biology 241(4):919 . ISSN 0022-5193. URL http://www.sciencedirect.com/science/article/pii/S0022519306000403.

[19] M. J. Feigenbaum, 1978. "Quantitative universality for a class of nonlinear transformations". Journal of Statistical Physics 19(1):25. ISSN 1572-9613. URL https://doi.org/10.1007/BF01020332.

[20] P. Vilela, D. Vasquez, 2016. "The effects of fluid motion on oscillatory and chaotic fronts". The European Physical Journal Special Topics 225:2563.

[21] A. Malevanets, et al., 1995. "Biscale chaos in propagating fronts". Phys. Rev. E 52:4724. URL https://link.aps.org/doi/10.1103/PhysRevE.52.4724.

[22] W. H. Press, et al., 2007. Numerical Recipes 3rd Edition: The Art of Scientific Computing. Cambridge University Press, USA, 3 edición. ISBN 0521880688.

[23] R. M. May, 1976. "Simple mathematical models with very complicated dynamics". Nature 261(5560):459. ISSN 1476-4687. URL https://doi.org/10.1038/261459a0.

[24] R. S. Spangler, B. F. Edwards, 2003. “Poiseuille advection of chemical reaction fronts: Eikonal approximation”. The Journal of Chemical Physics 118(13):5911–5915.

Appendix A

Code used

A.1 Stationary fronts

Shooting method for v and c free parameters

```
      program shooting
            real*8 xc, xv, f1, f2, f1v, f2v, f1c, f2c
            real*8 deltac, deltav, J11, J12, J21, J22
            real*8 xcd, xvd, L, vm, dL,Li,Lf
            real*8 xxc, xxv, difc, difv,b, bi,db
            integer iters, cont, i, N,N1,M
            character letter*1
            b=0.50d0
            Li=8.0d0
            Lf=5.0d0
            vm=0.d0
            xv = -0.455135734016744 06
            xc= 0.923204096064978 66
```

```
        dL=0.0010d0
        db=0.0010d0
        N=abs(Lf-Li)/dL
        M=b/db
        print*, M
        L=Li
!ajustando para beta
do i=0, M
        bi=db*i
900     iters = 0
        deltav = 1.0E-04
        deltac = 1.0E-04
        xcd =  xc+deltac
        xvd =  xv+deltav
        call shoot(xc, xv, f1, f2, L, vm,bi)
        call shoot(xcd, xv, f1c, f2c, L, vm,bi)
        call shoot(xc, xvd, f1v, f2v, L, vm,bi)
300     iters = iters + 1
        J11 = (f1v-f1)/deltav
        J12 = (f1c-f1)/deltac
        J21 = (f2v-f2)/deltav
        J22 = (f2c-f2)/deltac
        call NRG(f1, f2, J11, J12, J21, J22, xv, xc, deltav,
```

```
        xcd =  xc+deltac
        xvd =  xv+deltav
        call shoot(xc, xv, f1, f2, L, vm,bi)
        call shoot(xcd, xv, f1c, f2c, L, vm,bi)
        call shoot(xc, xvd, f1v, f2v, L, vm,bi)
        difc = abs(deltac)
        difv = abs(deltav)
        if ((difc.GT.1.0E-09).AND.(difv.GT.1.0E-09))go to 300
        end do
        print*, bi,xc,xv
!para L
        open(unit=1, file='8a10inestablebeta05parte2.dat')
!forward
do i=0, N
        L=Li-dL*i
800   iters = 0
        deltav = 1.0E-04
        deltac = 1.0E-04
        xcd =  xc+deltac
        xvd =  xv+deltav
        call shoot(xc, xv, f1, f2, L, vm,b)
        call shoot(xcd, xv, f1c, f2c, L, vm,b)
        call shoot(xc, xvd, f1v, f2v, L, vm,b)
```

```
500    iters = iters + 1
       J11 = (f1v-f1)/deltav
       J12 = (f1c-f1)/deltac
       J21 = (f2v-f2)/deltav
       J22 = (f2c-f2)/deltac
       call NRG(f1, f2, J11, J12, J21, J22, xv, xc, deltav,
       xcd =  xc+deltac
       xvd =  xv+deltav
       call shoot(xc, xv, f1, f2, L, vm,b)
       call shoot(xcd, xv, f1c, f2c, L, vm,b)
       call shoot(xc, xvd, f1v, f2v, L, vm,b)
       difc = abs(deltac)
       difv = abs(deltav)
       if ((difc.GT.1.0E-09).AND.(difv.GT.1.0E-09))go to 500
        write(1,*) L, xc, xv, f1,f2
       end do
       close(unit=1)
       end program
       subroutine shoot(cc, v, u, w, xL, vmf,b)
       real*8  cc, v, u, w, h, dx, hp, up, vp, wp, v0,b
       real*8  xx, vmf, xL, vz
       integer i
       h=1.0
```

```
      u=0.
      w=0.
      v0 = v
      dx = xL/10000.
      do 100 i=1,10000
      xx = dfloat(i)*dx
      hp=h+dx*u
      up=u+dx*v
      vp=v+dx*w
      wp=w+dx*(-v+(u**2)/2.-cc+b*w)
      u=up
      h=hp
      v=vp
      w=wp
100   continue
      v =v0
      end
      subroutine NRG(f,g,dfdx,dfdy,dgdx,dgdy,x,y,deltax,del
      real*8 f, g, dfdx, dfdy, dgdx, dgdy, x, y, deltax, de
      real*8 xn, yn
      um = -1./(dfdx*dgdy-dfdy*dgdx)
      deltax = um*(dgdy*f-dfdy*g)
      deltay = um*(dfdx*g-dgdx*f)
```

```
xn = x + deltax
yn = y + deltay
x = xn
y = yn
end program
```

Similar to the one used considering external flow.

A.2 Oscillatory fronts

Velocity vs time

```
program kshtiempovelocidad
implicit none
integer, parameter:: n=8, time=1000, x=100
doubleprecision, parameter:: dt=0.001, L=9.0210d0
doubleprecision, dimension(0:n)::Hn, Hi
doubleprecision, dimension(0:x)::Hx
doubleprecision, dimension(0:50000,0:1):: Vt
integer:: i, j, k, m, o,p, b, la
doubleprecision:: dx, q, rndm, delta, prom=0
m=time/dt
dx=L/x
q=3.141592/L
Hx=0.0d0
Hn=0.0d0
```

```
Hi=0.0d0
la=0
Hn(0)=12670.888715342826
Hn(1)=1.4492858461081681
Hn(2)=1.3564814802453244
Hn(3)=-1.2872635106138322
Hn(4)=7.3254558795586677E-002
Hn(5)=9.6451824504625472E-002
Hn(6)=-3.6753866019227782E-002
Hn(7)=3.6249267654035440E-004
Hn(8)=2.7852048907584265E-003
do i=1, 500000
        Hi=0.0d0
        do k=0, n
            Hi(0)=Hi(0)+(k*Hn(k))**2
        end do
        Hi(0)=dt*(Hi(0)*(q**2)*0.25)+Hn(0)
        do j=1,n
            do o=1, n
                do p=1, n
                    delta=0.
                    if(j.EQ.abs(o-p))then
                        delta=1.
```

```
                    end if
                    if(j.EQ.(o+p))then
                        delta=-1.
                    end if
                    Hi(j)=Hi(j)+o*Hn(o)*Hn(p)*p*delta
                end do
            end do
            Hi(j)=q**2*Hi(j)*0.25+(q*j)**2*Hn(j)-(j*q)**4
            Hi(j)=Hi(j)*dt+Hn(j)
        end do
        Hn=Hi
    end do
    do i=1, 500000
        Hi=0.0d0
        do k=0, n
            Hi(0)=Hi(0)+(k*Hn(k))**2
        end do
        Hi(0)=dt*(Hi(0)*(q**2)*0.25)+Hn(0)
        do j=1,n
            do o=1, n
                do p=1, n
                    delta=0.
                    if(j.EQ.abs(o-p))then
```

```
                    delta=1.
                end if
                if(j.EQ.(o+p))then
                    delta=-1.
                end if
                Hi(j)=Hi(j)+o*Hn(o)*Hn(p)*p*delta
            end do
        end do
        Hi(j)=q**2*Hi(j)*0.25+(q*j)**2*Hn(j)-(j*q)**4
        Hi(j)=Hi(j)*dt+Hn(j)
    end do
    if(MOD(i,10).EQ.0)then
        Vt(la,0)=i*dt
        Vt(la,1)=(Hi(0)-Hn(0))/dt
        la=la+1
    end if
    Hn=Hi
  end do
  open(unit=1, file='datos1.dat')
  do i=0, la-1
      write(1,*) Vt(i,0), Vt(i,1)
  end do
end program
```

Calculating maximum and minimum velocity for an interval of L

```
        program kshtiempovelocidad
implicit none

integer, parameter:: n=8, time=1000, x=100, nm=650
doubleprecision, parameter:: dt=0.0010d0, dL=0.010d0, Li=
doubleprecision, dimension(0:n)::Hn, Hi
doubleprecision, dimension(0:x)::Hx
doubleprecision, dimension(0:30000):: Vt
doubleprecision, dimension(0:nm,0:1,0:10000):: Vmm
doubleprecision, dimension(0:nm,0:n):: Hts
integer:: i, j, k, m, o,p, b, la, ij
integer, dimension(0:500000):: contador
doubleprecision:: dx, q, rndm, delta, L
m=time/dt
Vmm=0
Hn=0
contador=0
call srand(1000000)
do i=0, n
    rndm=rand()
    Hn(i)=rndm*0.1
end do
```

```
do ij=0, nm
L=Li+ij*dL
dx=L/x
q=3.141592/L
Hx=0.0d0
Hi=0.0d0
Vt=0
la=0
do i=1, 300000
        Hi=0.0d0
        do k=0, n
          Hi(0)=Hi(0)+(k*Hn(k))**2
        end do
        Hi(0)=dt*(Hi(0)*(q**2)*0.25)+Hn(0)
        do j=1,n
            do o=1, n
                do p=1, n
                  delta=0.
                  if(j.EQ.abs(o-p))then
                      delta=1.
                  end if
                  if(j.EQ.(o+p))then
                      delta=-1.
```

```
                    end if
                    Hi(j)=Hi(j)+o*Hn(o)*Hn(p)*p*delta
                end do
            end do
            Hi(j)=q**2*Hi(j)*0.25+(q*j)**2*Hn(j)-(j*q)**4
            Hi(j)=Hi(j)*dt+Hn(j)
        end do
        Hn=Hi
    end do
    do i=0,n
        Hts(ij,i)=Hn(i)
    end do
    print*, "a"
    do i=1, 300000
        Hi=0.0d0
        do k=0, n
            Hi(0)=Hi(0)+(k*Hn(k))**2
        end do

        Hi(0)=dt*(Hi(0)*(q**2)*0.25)+Hn(0)
        do j=1,n
            do o=1, n
                do p=1, n
```

```
                delta=0.
                if(j.EQ.abs(o-p))then
                    delta=1.
                end if
                if(j.EQ.(o+p))then
                    delta=-1.
                end if
                Hi(j)=Hi(j)+o*Hn(o)*Hn(p)*p*delta
            end do
        end do
        Hi(j)=q**2*Hi(j)*0.25+(q*j)**2*Hn(j)-(j*q)**4
        Hi(j)=Hi(j)*dt+Hn(j)
    end do
    if(MOD(i,10).EQ.0)then
        Vt(la)=(Hi(0)-Hn(0))/dt
        la=la+1
    end if
    Hn=Hi
end do
print*, ij, la
Vmm(ij,0,0)= L
do i=1, la-2
    if((Vt(i).GE.Vt(i+1)).AND.(Vt(i).GE.Vt(i-1)))then
```

```
            Vmm(ij,1,contador(ij))=Vt(i)
            contador(ij)=contador(ij)+1
        end if
        if((Vt(i).LE.Vt(i+1)).AND.(Vt(i).LE.Vt(i-1)))then
            Vmm(ij,1,contador(ij))=Vt(i)
            contador(ij)=contador(ij)+1
        end if
        if((Vt(i).EQ.Vt(i+1)).AND.(Vt(i).EQ.Vt(i-1)))then
            go to 140
        end if
    end do
140 continue
    end do
    open(unit=1, file='datosL95.dat')
    do i=0, nm
        do j=0, contador(i)-1
        write(1,*) Vmm(i,0,0), Vmm(i,1,j)
        end do
    end do
    close(unit=1)
    open(unit=3, file='coeffourierL95.dat')
    do i=0, nm
```

```
        do j=0,n
            write(3,*) Li+i*dL,j,Hts(i,j)
        end do
    end do
    close(unit=3)
end program
```

The programs used for external flow were similar.

Phase space diagrams

```
            program espaciofasesatractor
    implicit none

    integer, parameter:: n=8, x=100, posi=100
    doubleprecision, parameter:: L=9.010d0, dt=0.001
    doubleprecision, dimension(0:n)::Hn
    doubleprecision, dimension(0:n)::Hi
    doubleprecision, dimension(0:x)::Hx

    doubleprecision, dimension(0:30000,0:1)::Vt
    doubleprecision:: dx, q, delta, prom=0
    integer::la, i, j, o, p, b,k
    Hn=0
    q=3.141592/L
    dx=L/x
```

```
la=0
Hx=0
Hn(0)=58549.738354858324
Hn(1)=-0.91057914253127992
Hn(2)=2.0126480954039532
Hn(3)=-0.328039682528571O2
Hn(4)=-0.25533357944337931
Hn(5)=3.4446796999484448E-002
Hn(6)=1.4832733945615141E-002
Hn(7)=-3.427327045792613 6E-003
Hn(8)=-8.2309486696979870E-004
Hi=0
Vt=0
      do i=0, 300000
            Hi=0.0d0
            do k=0, n
                  Hi(0)=Hi(0)+(k*Hn(k))**2
            end do
            Hi(0)=dt*(Hi(0)*(q**2)*0.25)+Hn(0)
            do j=1,n
                  do o=1, n
                        do p=1, n
                              delta=0.
```

```
                if(j.EQ.abs(o-p))then
                    delta=1.
                end if
                if(j.EQ.(o+p))then
                    delta=-1.
                end if
                Hi(j)=Hi(j)+o*Hn(o)*Hn(p)*p*delta
            end do
        end do
        Hi(j)=q**2*Hi(j)*0.25+(q*j)**2*Hn(j)-(j*q)**4
        Hi(j)=Hi(j)*dt+Hn(j)
    end do
    if(MOD(i,10).EQ.0)then
        Vt(la,1)=(Hi(0)-Hn(0))/dt
        prom=0
        do b=0, x
            do j=0, n
                Hx(b)=Hx(b)+Hn(j)*cos(j*q*b*dx)
            end do
            prom=prom+Hx(b)
        end do
        do j=1,10
        prom=prom/x
```

```
            do b=0, x
                Hx(b)=Hx(b)-prom

            end do
            prom=0.0d0
            do b=0, x
                prom=prom+Hx(b)

            end do

            end do

            Vt(la,0)=Hx(posi)

            print*, la,Vt(la,0),Vt(la,1)
            la=la+1
        end if
        Hx=0
        Hn=Hi
end do
open(unit=1, file='espaciofasesL901sinflujx100.dat')
do i=0,la-2
```

```
        write(1,*) Vt(i,0),Vt(i,1)
    end do
    close(unit=1)
end program
```

The code used for the phase space diagrams, the code including external flow is similar.